Biomedical Physics & Engineering Express

ENDORSED BY IPEM Institute of Physics and Engineering in Medicine

PAPER

NCINM: organ dose calculator for patients undergoing nuclear medicine procedures

To cite this article: Daphnée Villoing *et al* 2020 *Biomed. Phys. Eng. Express* **6** 055010

Biomedical Physics & Engineering Express

PAPER

NCINM: organ dose calculator for patients undergoing nuclear medicine procedures

Daphnée Villoing[1,3], **Thomas A Cuthbert**[1,2], **Cari M Kitahara**[1] and **Choonsik Lee**[1,3]

[1] Division of Cancer Epidemiology and Genetics, National Cancer Institute, National Institutes of Health, Rockville, MD, United States of America
[2] Graduate School of Biomedical Sciences, University of Texas Health San Antonio, San Antonio, TX, United States of America
[3] Authors to whom any correspondence should be addressed.

E-mail: daphnee.villoing@nih.gov **and** leechoonsik@mail.nih.gov

RECEIVED
20 April 2020

REVISED
1 July 2020

ACCEPTED FOR PUBLICATION
8 July 2020

PUBLISHED
20 July 2020

Keywords: nuclear medicine, Monte Carlo radiation transport, computational human phantoms, organ absorbed dose

Supplementary material for this article is available online

Abstract

Nuclear medicine is the second largest source of medical radiation exposure to the general population after computed tomography imaging. Informed decisions regarding the use of nuclear medicine procedures require a better understanding of the magnitude of radiation dose and associated health risks. However, existing model-based organ dose estimation tools rely on simplified human anatomy models or commercial programs. Therefore, we developed a publicly-available dose calculation tool based on more sophisticated human anatomy models. We calculated a comprehensive library of photon and electron specific absorbed fractions (SAF) for multiple combinations of source and target regions within a series of pediatric and adult computational human phantoms matching the International Commission on Radiological Protection (ICRP)'s reference data, combined with a Monte Carlo radiation transport code. Then, we derived a library of S values from these SAFs and the nuclear decay data from ICRP Publication 107. Finally, we created a graphical user interface, named National Cancer Institute Dosimetry System for Nuclear Medicine (NCINM), to facilitate the dosimetry process. Approximately 13 million S values were derived from 2 million SAFs computed in this work. Comprehensive comparisons were conducted at different steps of the dosimetry chain with data available in software OLINDA/EXM 1.0 and IDAC 2.1. For instance, median ratios of photon self-absorption SAFs available from OLINDA/EXM 1.0 and IDAC 2.1 to those calculated in this study were 1.3 (interquartile range = 1.1–1.6) and 1.0 (interquartile range = 0.98–1.0), respectively. SAF differences between NCINM and OLINDA/EXM 1.0 were explained by the large inter-phantom anatomical variability. Our results illustrate the importance of realistic human anatomy models for use in dosimetry software. More phantoms and radionuclides, as well as a biokinetic module, will soon be added. Applications of the NCINM program include computation of absorbed doses for use in radiation epidemiologic studies and patient dose monitoring in nuclear medicine.

1. Introduction

With the advent of singlephoton emission computed tomography (SPECT) and positron emission tomography (PET) combined with computed tomography (CT) (Maurer 2008), new cardiac nuclear myocardial perfusion imaging systems (Hung *et al* 2016), and novel radiopharmaceuticals (Chiavassa *et al* 2006, Gutfilen and Valentini 2014), exponential growth in nuclear medicine procedures has been observed in recent decades in the United States (NCRP 2009, 2019). Annual per capita effective doses from nuclear medicine procedures doubled between 1980 (0.14 mSv) and 2016 (0.32 mSv), placing nuclear medicine as the second largest source of medical radiation exposure to the general population after CT (~1.5 mSv in 2016) (NCRP 2009, 2019). Quantifying the long-term health of this growing source of radiation exposure requires accurate estimation of radiation dose delivered to radiosensitive organs.

Depending on the availability of patient images and the accuracy required in dosimetry, two approaches have been developed, both based on the Medical Internal Radiation Dosimetry (MIRD) formalism (Loevinger *et al* 1991). The first approach, called a model-based dosimetry method, consists of the biokinetic data of a given radiopharmaceutical combined with organ dose conversion coefficients, called S values, computed from computational human phantoms combined with Monte Carlo radiation transport methods. IDAC (Johansson 1985), MIRDOSE (Stabin 1996), and OLINDA/EXM 1.0 (Stabin *et al* 2005) are the dose calculation tools using the model-based dosimetry approach, and these have been widely used in the scientific and clinical community. However, the dosimetric accuracy achieved by this approach depends substantially on the anatomical precision of computational human phantoms. These early dose calculators were based on computational phantoms, called stylized phantoms (Cristy 1980), in which anatomical structures were described by simple mathematical equations. With the introduction of more realistic computational phantoms (Xu 2014), starting from voxel phantoms and later hybrid phantoms, the use of stylized phantoms for internal dosimetry had been reported to significantly underestimate organ absorbed doses compared to realistic phantoms (Chao and Xu 2001, Yoriyaz *et al* 2001, Zankl *et al* 2003, Lee *et al* 2007, Lamart *et al* 2011, Marcatili *et al* 2015). By replacing the stylized phantoms in OLINDA/EXM 1.0 with more realistic hybrid phantoms, OLINDA/EXM 2.0 was introduced (Stabin and Farmer 2012). IDAC was also updated (Andersson *et al* 2014) using the data from ICRP Publication 133 (ICRP 2016), which is based on the reference adult male and female voxel phantoms (ICRP 2009). Another approach, called a patient-specific dosimetry method, derives the biokinetics of a given radiopharmaceutical and S values directly from the patients' scintigraphic and computed tomography image sets, respectively (Botta *et al* 2013, Marcatili *et al* 2015). The most accurate internal dosimetry now can be achieved by a full Monte Carlo simulation using both functional and anatomical 3D imaging. Such an approach nonetheless requires extensive time and expertise in image processing and Monte Carlo simulation methods, even when assisted by a graphical user interface (GUI), such as OEDIPE (Chiavassa *et al* 2006, Petitguillaume *et al* 2014).

Due to the challenges of accessing anatomical or functional images of patients for dosimetry, the patient-specific dosimetry method may not be appropriate for the large-scale dose reconstruction needed in epidemiological studies of radiation-associated health risks. A large epidemiological study of patients treated for hyperthyroidism conducted at the National Cancer Institute adopted the model-based dosimetry method. The original study by Ron *et al* (Ron *et al* 1998) used the stylized phantom-based S values (ICRP 1988) for organ dose calculations. Later, the study team found that these S values were systemically lower than those from realistic computational human phantoms (Lamart *et al* 2016). To improve the accuracy of the cohort dosimetry, a comprehensive set of ^{131}I S values were calculated using reference adult voxel phantoms combined with Monte Carlo radiation transport methods (Lamart *et al* 2016), and then used to compute absorbed doses for 17 organs and tissues (Melo *et al* 2015). These updated estimates were then used to quantify the dose-dependent relationships between ^{131}I and site-specific cancer mortality in patients treated for hyperthyroidism (Kitahara *et al* 2019). In the current study, we extended our S value database previously calculated for ^{131}I use in adults (Lamart *et al* 2016) to include a wider range of radionuclides and pediatric computational human phantoms. With the pediatric and adult S values combined, we created a graphical user interface (GUI)-based software, named the National Cancer Institute Dosimetry System for Nuclear Medicine (NCINM), to facilitate organ dose calculations. We conducted extensive comparisons of our results with existing model-based dosimetry tools.

2. Material and methods

NCINM is based on the widely-acknowledged MIRD formalism (Loevinger *et al* 1991). We developed this program in three steps. First, we calculated a comprehensive library of specific absorbed fractions (SAFs) for multiple combinations of source and target regions within a series of pediatric and adult computational human phantoms combined with a Monte Carlo radiation transport code. Second, we derived a library of S values from the SAFs and the nuclear decay data from ICRP Publication 107 (ICRP 2008a). Finally, we created a GUI-based program to facilitate the dosimetry process. Details will be presented in the following sections.

2.1. Computational human phantom series

We employed a series of computational human phantoms developed in a collaboration between the University of Florida and the National Cancer Institute (Lee *et al* 2010). The phantom series includes male and female pediatric and adult phantoms, representing the reference newborn, 1-, 5-, 10-, and 15-year-old, and adults. The anatomy of the phantoms match the reference data from ICRP Publication 89 (ICRP 2002) and the reference data on the alimentary tract from ICRP Publication 100 (ICRP 2006). The tissue densities and elemental compositions were obtained from the reference data reported in ICRP Publication 89 and Report 46 (ICRU 1992) by the International Commission on Radiation Units (ICRU). The original phantoms were created in non-uniform rational B-spline (NURBS) and polygon mesh format and were

Table 1. (A). List of 68 source regions considered in the calculation of specific absorbed fractions (L = Left, R = Right, LR = Left and Right, ET = Extrathoracic, LN = Lymph nodes, RECT = Rectosigmoid). (B). List of 55 target regions considered in the calculation of specific absorbed fractions (RECT = Recto-sigmoid, L = Left, R = Right, ET = Extrathoracic, LN = Lymph nodes, RECT = Rectosigmoid).

Adipose	Esophagus	Lymph Nodes ET	Thyroid
(A)			
Adrenal L	ET2	LN but ET/Thoracic	Tongue
Adrenal R	Gall Bladder Content	LN Thoracic	Tonsils
Adrenal LR	Gall Bladder Wall	Muscle	Trabecular Bone Marrow[c]
Blood Body	Gonads: Testes or Ovaries	Nasal Anterior	Trabecular Bone Mineral[d]
Blood Heart	Heart Wall	Nasal Posterior	Ureters
Blood Body + Heart	Kidney L	Oral Cavity	Urinary Bladder Content
Brain	Kidney L Cortex	Pancreas	Urinary Bladder Wall
Breast Adipose + Glandular	Kidney L Medulla	Pituitary Gland	
Breast Adipose	Kidney L Pelvis	Prostate or Uterus	
Breast Glandular	Kidney R	Salivary Glands	
Bronchi	Kidney R Cortex	Skin	
Colon L Content	Kidney R Medulla	Small Intestine Content	
Colon L Wall	Kidney R Pelvis	Small Intestine Wall	
Colon R Content	Kidney LR	Spinal Cord	
Colon R Wall	Lenses of Eye	Spleen	
Colon RECT Content	Liver	Stomach Content	
Colon RECT Wall	Lung L	Stomach Wall	
Cortical Bone Marrow[a]	Lung R	Teeth	
Cortical Bone Mineral[b]	Lung LR	Thymus	
(B)			
Adipose	Kidney Cortex L	Prostate or Uterus	
Adrenal	Kidney cortex R	Salivary Glands	
Adrenal L	Kidney Medulla L	Skin	
Adrenal R	Kidney Medulla R	Small Intestine Wall	
Bronchi	Kidney Pelvis L	Spinal Cord	
Brain	Kidney Pelvis R	Spleen	
Breast Adipose	Lenses of Eye	Stomach Wall	
Breast Glandular	Liver	Thymus	
Colon Wall	Lung	Thyroid	
Colon RECT Wall	Lung L	Tongue	
Colon Wall L	Lung R	Tonsils	
Colon Wall R	LN ET	Ureters	
Esophagus	LN but ET/Thoracic	Urinary Bladder Wall	
ET Region	LN Thoracic	Active Marrow	
Gall Bladder Wall	Muscle	Shallow Marrow	
Gonads	Nasal Anterior		
Heart Wall	Nasal Posterior		
Kidney	Oral Mucosa		
Kidney R	Pancreas		
Kidney L	Pituitary Gland		

[a] Cortical bone marrow: The marrow contained in the medullary cavities in the shafts of the long bones.

[b] Cortical bone mineral: The mineral contained in the cortical regions of all bones.

[c] Trabecular bone marrow: The marrow contained in the spongiosa regions of all bones (marrow fraction of spongiosa bones).

[d] Trabecular bone mineral: The mineral in the spongiosa regions of all bones (mineral bone fraction of spongiosa bones).

converted to voxel format for Monte Carlo radiation transport simulations.

We selected source and target regions within the phantom anatomy following ICRP Publication 110 (ICRP 2009). Table 1(A) and (B) show the list of 68 source and 55 target regions considered in the current study, respectively.

2.2. Calculation of specific absorbed fractions

We calculated a comprehensive set of photon and electron absorbed fractions (AF), $\phi(r_T \leftarrow r_S)$, the fraction of the particle energy emitted from a source region r_S that is deposited in a target region r_T. We used a general-purpose Monte Carlo radiation transport code MCNPX version 2.7 (Pelowitz 2011) to simulate radiation transport within source regions and between source and target regions. Standard cross

section libraries were used, and the default energy cutoffs for electron transport of 1 keV were adopted. MCNPX tally *F8 was used to score energies (MeV) per source particle, and the transport of secondary electrons was taken into account. A total of 100 million particles were simulated for each source organ in order to keep Monte Carlo statistical errors below 1% in most combinations of source and target regions. Photon and electron AFs were computed for 25 different energies ranging from 10 keV to 6 MeV for each of the 12 pediatric and adult male and female computational phantoms for 68 source and 55 target regions, representing about 2 million AF values. The Biowulf High-Performance Computer available at the National Institutes of Health was used to conduct the large-scale Monte Carlo simulations. Next, we derived SAFs $\Phi(r_T \leftarrow r_S)$ (kg^{-1}) by dividing the AF values by the mass of a target organ m_{r_T}. To be consistent with the definition of organ mass in ICRP Publication 133, we derived the blood mass in each organ and tissue using the blood distribution in ICRP Publication 89 (ICRP 2002) and added them to the target region mass.

Alimentary tracts have thin radiosensitive layers which cannot be described using the voxel resolution like in the rest of this study. As an alternative, we replaced the SAFs for adult male and female alimentary tract computed from our voxel phantoms with the values published in ICRP Publication 133 (ICRP 2016), which are adopted from ICRP Publication 100. We kept the original values for the pediatric phantoms since pediatric SAFs for detailed alimentary tract are not yet available. The list of source and target regions adopted from ICRP Publication 133 includes the following pairs: SAF (Left Colon Wall ← Left Colon Contents), SAF (Right Colon Wall ← Right Colon Contents), SAF (Rectosigmoid Colon Wall ← Rectosigmoid Colon Contents), SAF (Esophagus Wall ← Esophagus Contents), SAF (Small Intestine Wall ← Small Intestine Contents), and SAF (Stomach Wall ← Stomach Contents).

2.3. Calculation of S values

S values (mGy/MBq-s) were derived from the photon and electron SAFs (kg^{-1}) using the following equation:

$$S(r_T \leftarrow r_S) = \sum_i n_i E_i \cdot \Phi(r_T \leftarrow r_S) \quad (1)$$

where n_i is the probability of emission of radiation type i at the emitted energy E_i of a given radionuclide, and $\Phi(r_T \leftarrow r_S)$ is the SAF for a source region r_S and a target region r_T. We adopted the nuclear decay data in ICRP Publication 107 (ICRP 2008a) for a total of 299 radionuclides out of Eckerman and Endo's selection of 333 radionuclides (Eckerman and Endo 2008) based on their relevance to diagnostic and therapeutic nuclear medicine procedures. ICRP Publication 107 provides information on physical half-lives, decay chains, and the yields and energies of radiation emitted in the nuclear transformations (ICRP 2008a). All monoenergetic emissions and main beta emissions were considered in the S value calculations; contribution from daughter nuclei were not taken into account.

Using an in-house MATLAB script, S values were calculated from the SAFs and the radionuclide-specific energy spectra for 12 phantoms, 299 radionuclides, 68 source regions, and 55 target regions. For skeletal dosimetry, we adopted a library of dose response function specified for a total of 30 different bone sites (Johnson *et al* 2011). The photon fluence was scored in the spongiosa regions in each bone site and multiplied by the dose response function, which converts photon fluence to absorbed dose delivered to the active and shallow bone marrows in each bone site. Next, we weighted bone site specific marrow doses by marrow distribution across the whole skeletons to derive whole body active and shallow marrow doses.

The process is summarized in the following equation:

$$Dr_T = \sum_x Dr_T(x) = \sum_x \left[f_{r_T}(x) \int_E \Phi(E, x)\mathcal{R}(r_T, E, x)dE \right] \quad (2)$$

where $\mathcal{R}(r_T, E, x)$ is the dose response function for the target tissue r_T (active bone marrow or shallow bone marrow), photon energy E, and the bone site x; $\Phi(E, x)$ is the fluence scored within the spongiosa region of bone site x at the energy of E; $f_{r_T}(x)$ is the fraction of the target tissue r_T within the bone site x; $Dr_T(x)$ is radiation dose deposited to the target tissue r_T within the bone site x; and Dr_T is radiation dose deposited to the target tissue r_T across the whole body.

The effective dose (tissue-weighted sum of the equivalent doses in all specified tissues and organs of the body) was also included in NCINM using two sets of tissue weighting factors from ICRP Publication 60 (ICRP 1991) and 103 (ICRP 2007).

2.4. Graphical user interface

Based on the library of S values, we developed a user interface to facilitate the input of parameters and the calculation of target region dose using a multi-platform computer language, Xojo (Xojo, Inc. Austin, TX). User input data include:

- Selection of the patient's gender: male or female;
- Selection of the patient's age: 0-, 1-, 5-, 10-, 15-years, or adult;
- Selection of the radionuclide out of 299;
- Manual input of the administered activity—either in MBq or mCi;
- Selection of the source regions out of 68 regions listed in table 1(A);
- Manual input of the biokinetic data: residence time (hour) or cumulated activities (MBq-s).

Table 2. Comparison of the features between OLINDA/EXM 1.0, OLINDA/EXM 2.0, IDAC 2.1 and NCINM.

Features	OLINDA/EXM 1.0	OLINDA/EXM 2.0	IDAC 2.1	NCINM
Type of the computational human phantoms used	Stylized	Hybrid	Voxel	Hybrid
Reference anatomical data	ICRP Publication 23	ICRP Publication 89	ICRP Publication 89	ICRP Publication 89
Pediatric phantoms included?	Yes	Yes	No	Yes
Availability of phantoms	Mathematical equations free	Commercial	Free	Free
Accessibility of the program	Commercial	Commercial	Free	Free

The following output will be displayed real-time:

- Absorbed doses (mGy) and absorbed doses per unit administered activity (mGy/MBq) for all target regions listed in table 1(B);
- Two effective doses (mSv) based on ICRP Publication 60 (ICRP 1991) and 103 (ICRP 2007),
- Target region mass;
- S values (mGy/MBq.s) for selected source and target regions, selected phantom, and selected radionuclide (downloadable in text format).

Absorbed doses per unit administered activity (mGy/MBq), $\frac{D(r_T)}{A_0}$, also called absorbed dose coefficients, to target region r_T were calculated using the following equation:

$$\frac{D(r_T)}{A_0} = \sum_{r_S} \frac{\tilde{A}(r_S)}{A_0} S(r_T \leftarrow r_S) \quad (3)$$

where $\frac{\tilde{A}(r_S)}{A_0}$ is the cumulated activity per unit administered activity (s) in source tissue r_S and $S(r_T \leftarrow r_S)$ is the S value for source region r_S and target region r_T.

Three automatic unit conversions (in both ways) were programmed to suit different user preferences and applications: the administered activity between MBq and mCi; between the residence time (hour) and cumulated activity (MBq-s) derived from the residence time and administered activity; and between the absorbed dose (mGy) derived from administered activity (MBq) and the absorbed dose per administered activity (mGy/MBq). Two panels for input and output were arranged in a single window to increase the efficiency of the dose calculation process. We also created a module to automatically calculate the absorbed dose for many patients in batch mode. Users can create a text file listing the input parameters, which will then be imported into NCINM: patient ID, patient age (0, 1, 5, 10, 15, and 35), patient gender ID (1 = female, 2 = male), radionuclide ID (1-299), administered activity (MBq), region ID for source #1 (1-69), residence time for source #1, region ID for source #2, residence time for source #2, region ID for source #3, residence time for source #3, etc. Output data as described above will be created in another text file.

We incorporated an organ mass scaling option in order for users to account for patient specific organ mass in dose calculations. Since the mass scaling is unnecessary for cross-fire SAFs (Petoussi-Henss *et al* 2007), we only provided this option for self-absorption. The mass of the target organ can be modified only when the same organ is selected as the source. The MIRD pamphlet 11 (Snyder *et al* 1975) recommends to scale photon SAFs by the two-third power of the mass, and electron SAFs by the inverse power of the mass. Such a scaling of SAFs would slow down performance of the software, hence a direct scaling of pre-calculated S values by the two-third power of the mass was implemented, despite a potential under-estimation of the electron contribution:

$$S(r_T \leftarrow r_S)_{patient} = S(r_T \leftarrow r_S)_{phantom} \times \left(\frac{m_{Tphantom}}{m_{Tpatient}}\right)^{2/3} \quad (4)$$

where $S(r_T \leftarrow r_S)_{patient}$ is a scaled S value for a given patient, $S(r_T \leftarrow r_S)_{phantom}$ is a pre-calculated S value from a corresponding phantom, $m_{Tphantom}$ is the target organ mass of the phantom, and $m_{Tpatient}$ is the target organ mass of the patient.

2.5. Comparison with the existing data

We compared our data with the existing values in each of the calculation steps described above. First, we compared the mass of eight major target organs (adrenals, brain, kidneys, pancreas, spleen, thymus, and thyroid) used in our calculations with the values used in OLINDA/EXM 1.0 (stylized pediatric and adult phantoms) and IDAC 2.1 (ICRP reference adult voxel phantoms). We did not include alimentary tract organs into comparisons because we adopted the detailed SAFs and thin layer mass from ICRP Publication 133. We assumed that OLINDA/EXM 1.0 adopted the stylized phantom series developed at the Oak Ridge National Laboratory and derived the organ mass from the ORNL report. Main differences between the software compared in the study—and OLINDA/EXM 2.0 to which we did not get access—are summarized in table 2.

Second, we compared our pediatric and adult SAFs with those from OLINDA/EXM 1.0. Assuming electron AFs in OLINDA/EXM 1.0 are unity for self-absorption, we derived electron self-absorption SAFs

from the target organ masses for comparison. We also compared our adult SAF data with those from IDAC 2.1, which was published in ICRP Publication 133 (ICRP 2016). For the sake of clarity, the SAFs from ICRP Publication 133 will be referred to as IDAC 2.1 SAFs hereafter. The comparison was restricted to the 12 energies ranging from 10 keV to 4 MeV available in OLINDA/EXM 1.0.

Third, we compared our pediatric and adult S values with those from OLINDA/EXM 1.0 across 36 different source and target region pairs among our eight organs of interest (adrenals, brain, kidneys, pancreas, spleen, thymus, and thyroid) and for seven radionuclides commonly used in nuclear medicine: ^{18}F and ^{68}Ga for PET and PET/CT imaging, ^{99m}Tc and ^{123}I for SPECT and SPECT/CT imaging, ^{131}I and ^{177}Lu for targeted radionuclide therapy (TRT), and ^{111}In for both imaging and therapy. We calculated the ratio of S values from OLINDA/EXM 1.0 to those from NCINM to evaluate differences.

Finally, we compared our adult absorbed doses per unit administered activity (mGy/MBq), also called absorbed dose coefficients, with those from OLINDA/EXM 1.0 (for pediatric and adult phantoms) and IDAC 2.1 (for adult phantoms only) across the eight organs of interest mentioned above and four radiopharmaceuticals commonly used in nuclear medicine: ^{111}In-DTPA-octreotide (Octreoscan^{TM}), a SPECT radiotracer used in the diagnostic of neuroendocrine tumors, ^{99m}Tc-MAG3, the main radiotracer used for renal imaging, ^{99m}Tc-ECD, a SPECT radiotracer used in brain imaging, and ^{18}F-FDG, the most common PET radiotracer used for brain and pancreas scans, tumor localization, and in cardiac procedures. The biokinetic data were obtained from ICRP Publications 53 (ICRP 1988), 80 (ICRP 1998), and 106 (ICRP 2008b) (table 3). Absorbed dose values were also provided in supplementary data is available online at stacks.iop.org/BPEX/6/055010/mmedia for the same four radiopharmaceuticals and with the same biokinetic data, using survey-based US typical administered activities (Drozdovitch *et al* 2015) to the adult male phantom. Administered activities to the pediatric phantoms were adjusted based on whole body mass. These activities were not calculated with clinical purpose and the resulting absorbed doses are provided only for benchmarking.

Table 3. Biokinetic data of ^{111}In-DTPA-octreotide, ^{99m}Tc-MAG3, ^{99m}Tc-ECD and ^{18}F-FDG.

^{111}In-DTPA-octreotide (ICRP 1998)	
Source organs	Residence times (h)
Kidneys	2.76
Liver	2.59
Spleen	2.3
Thyroid	0.05
Urinary bladder (cont)	
Adult and 15-y-old	1.65
10-y-old	1.4
5-y-old, 1-y-old, newborn	0.91
Other organs and tissues	6.9
^{99m}Tc-MAG3 (ICRP 1998)	
Source organs	Residence times (h)
Kidneys	0.07
Urinary bladder (content)	
Adult and 15-y-old	2.66
10-y-old	2.33
5-y-old, 1-y-old, newborn	1.6
Other organs and tissues	0.23
^{99m}Tc-ECD (ICRP 2008b)	
Source organs	Residence times (h)
Brain	
Adult	0.3
15-y-old	0.5
10-y-old	0.84
5-y-old	1.1
1y-old, newborn	1.4
Colon (content), left	0.32
Colon (content), right	0.41
Colon (content), rectosigmoid	0.12
Gallbladder (content)	0.19
Kidneys	0.13
Liver	0.27
Lungs	0.08
Small intestine (content)	0.44
Thyroid	0.01
Urinary bladder (content)	
Adult, 15-y-old	1.2
10-y-old	1.1
5-y-old	0.92
1-y-old, newborn	0.58
Other organs and tissues	
Adult	1.8
15-y-old	1.7
10-y-old	1.5
5-y-old	1.3
1-y-old, newborn	1.1
^{18}F-FDG (ICRP 2008b)	
Source organs	Residence times (h)
Brain	0.21
Heart (wall)	0.11
Liver	0.13
Lungs	0.08
Urinary bladder (content)	
Adult, 15-y-old, 10-y-old	0.26
5-y-old	0.23
1-y-old, newborn	0.16
Other organs and tissues	1.7

3. Result and discussion

3.1. Organ mass comparison

The organ mass from OLINDA/EXM 1.0 based on the ORNL stylized phantoms is overall smaller (up to 50% for the pancreas) than that of NCINM. The organ mass from NCINM and IDAC 2.1 are nearly identical since both adopt the ICRP reference data and blood-inclusive target organ mass. The organ mass data in the ICRP Publication 89 (ICRP 2002), adopted in the

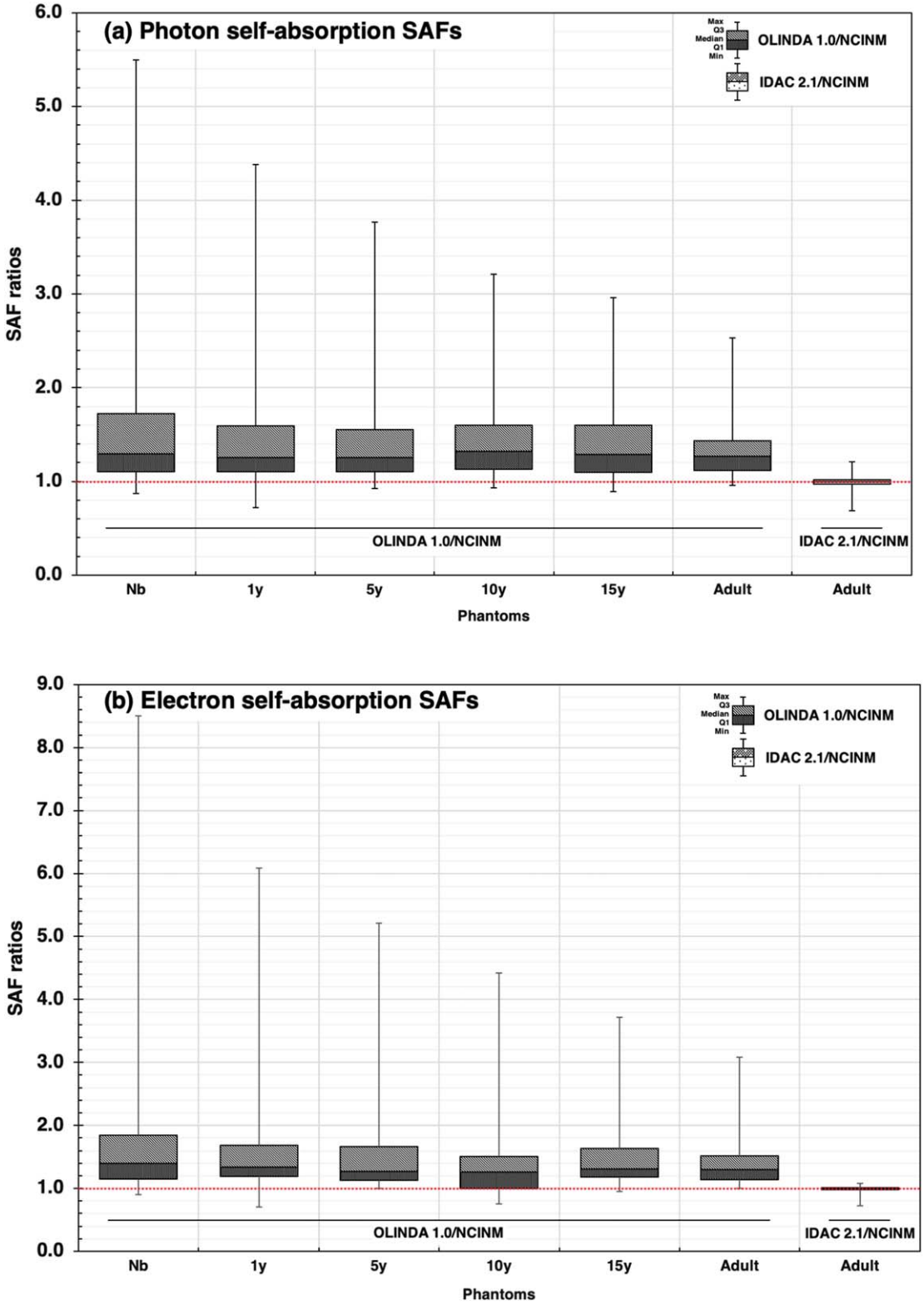

Figure 1. The ratios of (a) photon and (b) electron self-absorption specific absorbed fractions between OLINDA/EXM 1.0 and NCINM for adult and pediatric phantoms and between IDAC 2.1 and NCINM for adult phantoms, across twelve energies from 10 keV to 4 MeV and eight organs of interest.

development of the UF/NCI phantoms and the ICRP reference adult phantoms, do not include blood mass. Therefore, we added the blood mass to the target organ mass to simulate realistic human anatomy, which is also the case of ICRP Publication 133 (ICRP 2016) adopted in IDAC 2.1. On the contrary, blood mass was not added to the mass of source organs since blood is considered as a separate source region in the biokinetic models.

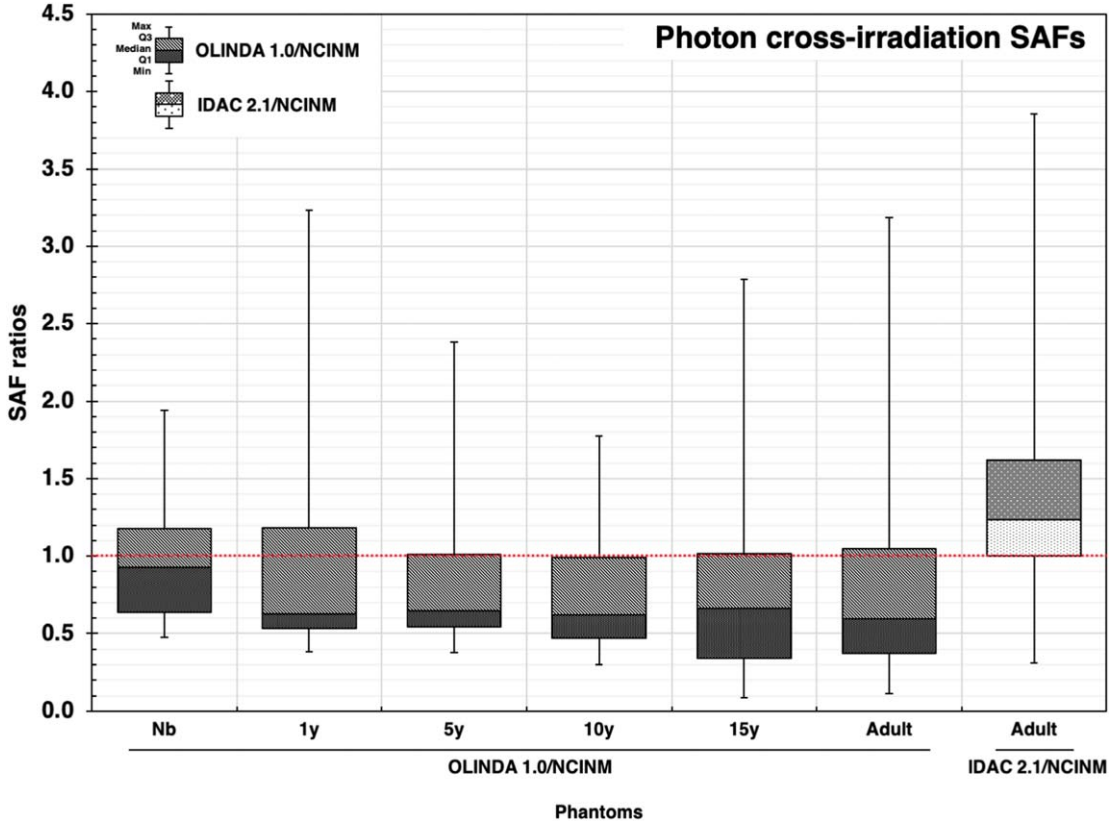

Figure 2. The ratios of cross-irradiation specific absorbed fractions for 100 keV photons from OLINDA/EXM 1.0 to those from NCINM for pediatric and adult phantoms. The comparison between IDAC 2.1 and NCINM was conducted only for adult phantoms.

3.2. Specific absorbed fractions

A comprehensive library of SAFs was created for photons and electrons, 25 energies, 12 pediatric and adult phantoms, 68 source regions, and 55 target regions. The full SAF library is available in the supplementary data (stacks.iop.org/BPEX/6/055010/mmedia).

Photon self-absorption SAFs from OLINDA/EXM 1.0 were overall greater than those from NCINM (figure 1(A)). The ratios (OLINDA/NCINM) varied from 0.72 to 5.5 (interquartile range (IQR) = 1.1–1.6; mean = 1.4; median = 1.3) across the eight organs, 12 phantoms, and 12 photon energies. Maximum differences increased with decreasing phantom ages. Much smaller differences were observed between IDAC 2.1 and NCINM, with SAF ratios varying from 0.69 to 1.2 (IQR = 0.97–1.0; mean = 0.98; median = 0.99) across the eight organs of interest, adult male and female phantoms and 12 photon energies.

Similar patterns were observed for electrons (figure 1(B)). Electron self-absorption SAFs from OLINDA/EXM 1.0 were overall greater than those from NCINM with the ratio (OLINDA/NCINM) ranging from 0.70 to 8.5 (IQR = 1.1–1.6; mean = 1.5; median = 1.3) across the eight organs, 12 phantoms, and 12 photon energies. Phantoms for younger ages show greater differences. The ratios of electron self-absorption SAFs from IDAC 2.1 to those from NCINM varied from 0.72 to 1.1 (IQR = 0.98–1.0; mean = 0.99; median = 1.0), which is much smaller than the difference from OLINDA/EXM 1.0.

Photon cross-irradiation SAFs at 100 keV from NCINM were compared with those from other programs (figure 2). The ratios (OLINDA/NCINM) varied from 0.09 to 3.2 (IQR = 0.49–1.1; mean = 0.84; median = 0.67) across the eight organs and 12 pediatric and adult phantoms. In comparison with IDAC 2.1, SAF ratios (IDAC/NCINM) varied from 0.31 to 3.9 (IQR = 1.0–1.6; mean = 1.4; median = 1.2) across the eight organs and adult male/female phantoms. Relatively greater difference was observed in SAF (thymus ← thyroid) in the 15-year-old phantoms, with ratios as small as 0.10.

Electron cross-irradiation SAFs were all set to zero in OLINDA/EXM 1.0 so that comparison with NCINM was not performed. The ratios (IDAC 2.1/NCINM) of electron cross-irradiation SAFs at 1 MeV varied from 0.10 to 510 (IQR = 1.6–3.5; mean = 33; median = 2.1) across the eight organs and two adult phantoms.

3.3. S values

A total of 13 million S values were derived for the 12 pediatric and adult phantoms, 299 radionuclides, 68 source, and 55 target regions from the photon and electron SAFs. S values for select source/target pairs and radionuclides (^{131}I, ^{99m}Tc, ^{123}I, ^{68}Ga, ^{18}F, ^{111}In and ^{177}Lu) are available in the supplementary data

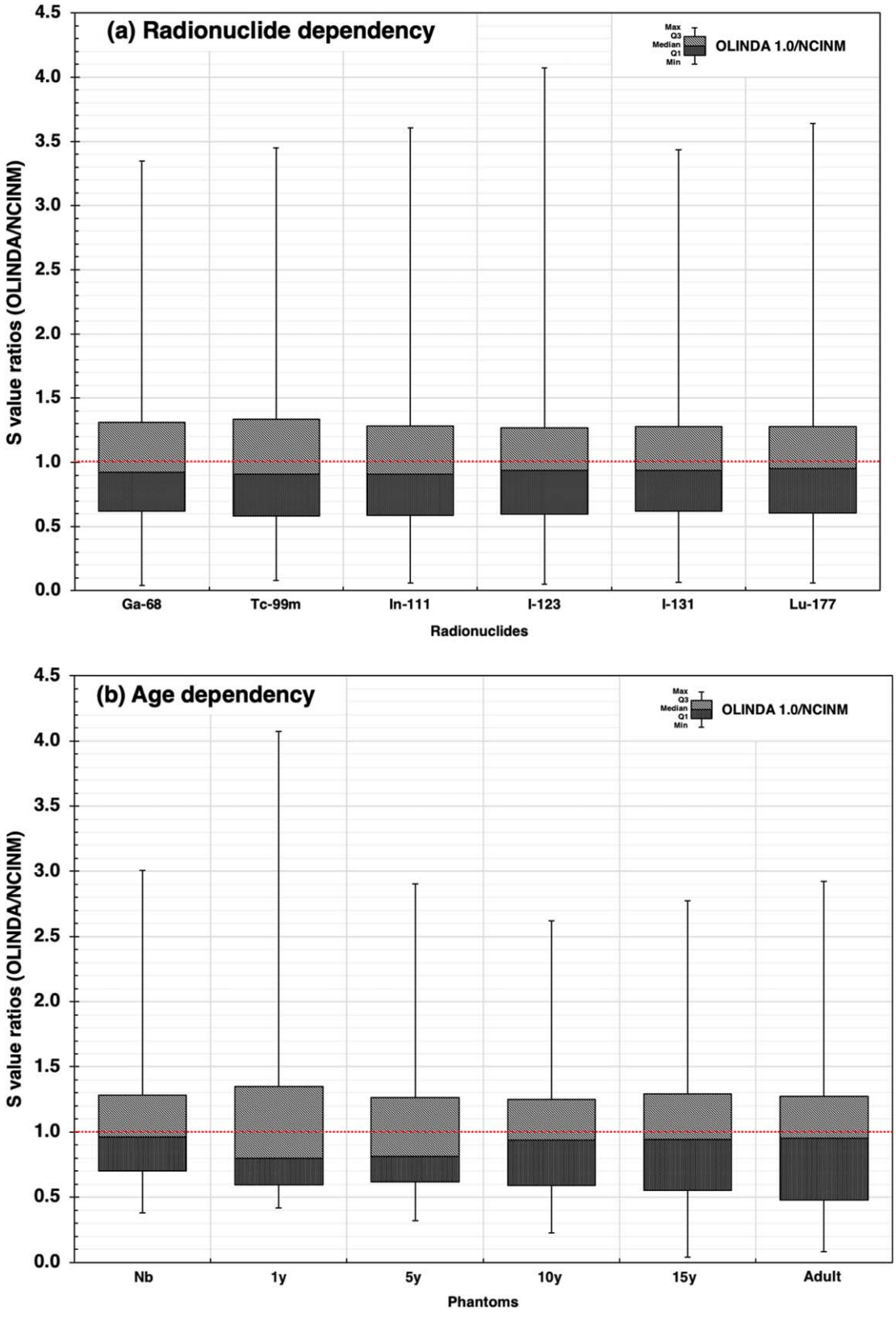

Figure 3. Ratios of the S values from OLINDA/EXM 1.0 to those from NCINM for thirty-six source/target pairs: (a) radionuclide dependency averaged over the 12 phantoms and (b) age dependency averaged over the seven radionuclides.

(stacks.iop.org/BPEX/6/055010/mmedia). The full library is accessible on the NCINM software. Radionuclide-dependent ratios (OLINDA/NCINM) of the S values averaged across all phantoms and source-target pairs varied from 0.04 to 4.1 (IQR = 0.60–1.3; mean = 1.0; median = 0.93) (figure 3(A)). Age-dependent ratios (OLINDA/NCINM) of S values varied from 0.55 to 3.0 (IQR = 1.2–1.5; mean = 1.4; median = 1.3) across the eight organs and seven radionuclides (figure 3(B)).

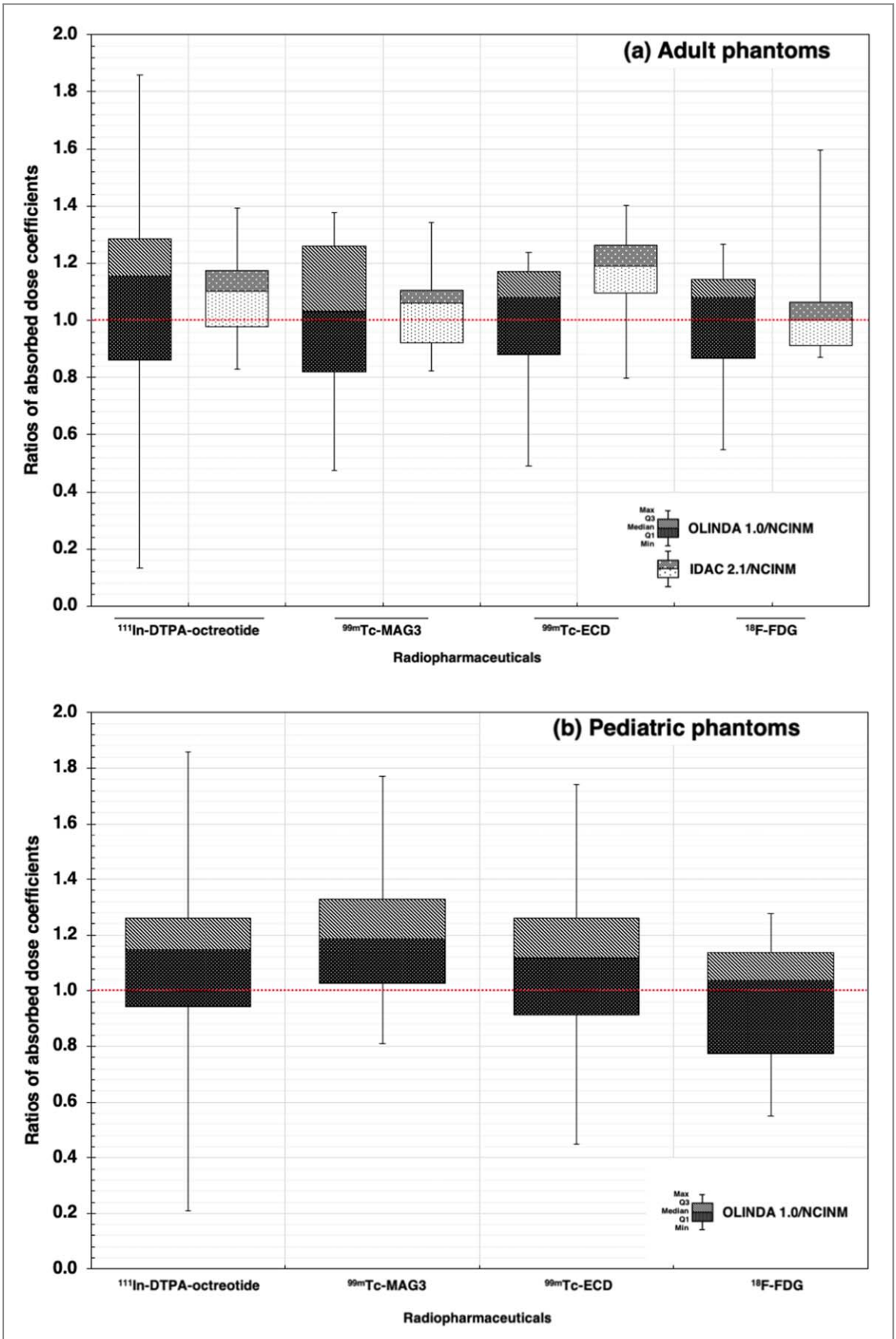

Figure 4. The ratios of absorbed dose coefficients (mGy/MBq) from OLINDA/EXM 1.0 and IDAC 2.1 to those from NCINM for four radiopharmaceuticals and eight target organs: (a) the eight pediatric male and female phantoms and (b) the adult male and female phantoms.

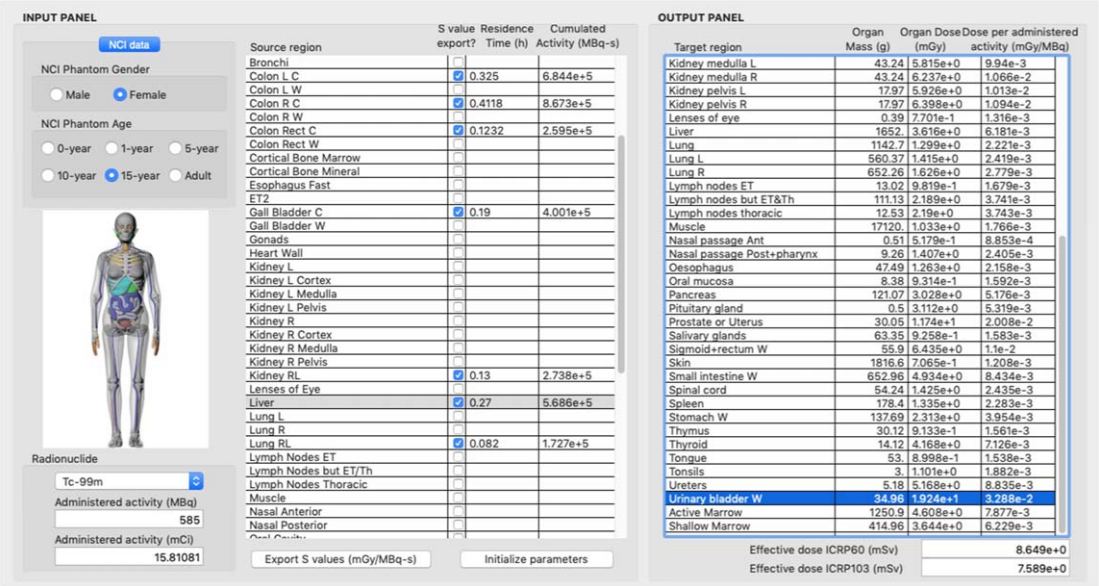

Figure 5. Graphical user interface of the NCINM program showing an example of dose calculation for the 15-year-old female phantom administered with 585 MBq of ^{99m}Tc-ECD.

3.4. Absorbed dose coefficients

Absorbed dose coefficients (mGy/MBq) for four common radiopharmaceuticals were calculated for the 12 phantoms and 55 target organs and are available from the supplementary data (stacks.iop.org/BPEX/6/055010/mmedia). For three radiopharmaceuticals, ^{99m}Tc-MAG3, ^{99m}Tc-ECD and ^{18}F-FDG, the urinary bladder wall showed the greatest absorbed dose coefficients in the adult phantom, which were 0.052, 0.026, and 0.053 mGy/MBq, respectively. In the case of ^{111}In-DTPA-octreotide, the thyroid (92 mGy/MBq) and spleen (0.43 mGy/MBq) received the greatest doses. Absorbed dose coefficients for younger age phantoms were overall greater than those for older age phantoms. For example, the absorbed dose coefficients to the urinary bladder wall after administration of ^{99m}Tc-ECD were 2 and 4 times greater for 5-year-old and newborn phantoms than those of the adult male phantom, respectively.

Ratio (OLINDA/NCINM) of absorbed dose coefficients for the pediatric phantoms from 0.43 to 1.8 (IQR = 0.91–1.2; mean = 1.1; median = 1.1) (figure 4(A)) and the ratio for the two adult phantoms varied from 0.14 to 1.4 (IQR = 0.86–1.2; mean = 1.0; median = 1.1) (figure 4(B)). The ratio (IDAC/NCINM) for the two adult phantoms varied from 0.58 to 1.8 (IQR = 0.97–1.2; mean = 1.1; median = 1.1) (figure 4(B)).

3.5. NCINM program

Figure 5 shows the graphical user interface of the NCINM program, where a comprehensive library of S values derived from the NCI phantom series combined with the energy spectra for a total of 299 radionuclides was incorporated. As an example, the information about a patient and administered activity was entered on the left panel: the 15-year-old female to which 585 MBq of ^{99m}Tc-ECD was administered (automatically converted to 15.8 mCi). The biokinetic data was inputted as shown in the middle panel and the resulting target organ doses (mGy) and dose per administered activity (mGy/MBq) are shown in the right panel with the mass of the 55 target regions. Two effective doses based on the ICRP Publication 60 and 103 are shown at the bottom of the right panel. Users can export S values for the selected source regions using the button, 'Export S values', at the bottom of the middle panel.

4. Discussion

This study was intended to develop a user-friendly organ dose calculation program for patients undergoing nuclear medicine procedures. We adopted the NCI voxel phantom series to resolve the underestimation of organ dose by the old stylized phantoms reported in many studies comparing old and new computational human phantoms (Chao and Xu 2001, Yoriyaz *et al* 2001, Zankl *et al* 2003, Lee *et al* 2007, Lamart *et al* 2011, Marcatili *et al* 2015). NCINM provides organ doses based on anatomically realistic computational human phantoms representing reference pediatric and adult males and females. We also incorporated several convenient features into the program to facilitate the use of the tool for epidemiological studies as well as clinical investigations.

We performed rigorous benchmarking comparisons with the existing dose calculation tools. Large differences observed in self-absorption SAFs between NCINM and OLINDA/EXM 1.0 are mainly attributed

Table 4. Mass (g) of the eight organs of interest in the adult and pediatric male and female phantoms used in NCINM, OLINDA/EXM 1.0, and IDAC 2.1.

	Newborn male			1-y-old male			5-y-old male			10-y-old male			15-y-old male		
	NCINM			NCINM			NCINM			NCINM			NCINM		
Organs	Source	Target	OLINDA	Source	Target	OLINDA	Source	Target	OLINDA	Source	Target	OLINDA	Source	Target	OLINDA
Adrenals	5.9	6.1	5.8	3.9	4.3	3.5	5.0	5.9	5.3	6.9	8.4	7.2	9.8	12.7	10.5
Brain	315.6	319.0	352.0	948.1	954.5	884.0	1246.1	1263.9	1260.0	1308.2	1338.7	1360.0	1416.4	1473.6	1410.0
Kidneys	26.3	32.0	23.0	73.4	84.0	62.9	115.9	145.6	116.0	189.3	240.2	173.0	263.5	358.9	248.0
Liver	129.9	158.6	121.0	329.0	382.0	292.0	570.6	719.0	584.0	828.0	1082.4	887.0	1302.0	1779.0	1400.0
Pancreas	6.0	7.7	2.8	19.9	23.1	10.3	35.0	43.9	23.6	60.0	75.2	30.0	109.0	137.6	64.9
Spleen	9.5	13.5	9.1	29.0	36.4	25.5	49.9	70.7	48.3	79.8	115.4	123.0	129.8	196.6	123.0
Thymus	13.0	13.0	11.0	16.1	16.1	22.9	30.1	30.1	29.6	37.3	37.3	28.4	35.2	35.2	28.4
Thyroid	1.3	1.5	1.3	1.8	2.1	1.8	3.4	4.3	3.5	7.9	9.4	12.4	12.0	14.9	12.4

	Adult male					Adult female				
	NCINM			IDAC		NCINM			IDAC	
Organs	Source	Target	OLINDA	Source	Target	Source	Target	OLINDA	source	target
Adrenals	13.6	17.0	16.0	14.0	17.0	12.9	15.0	14.0	13.0	16.0
Brain	1446.6	1514.0	1420.0	1450.0	1517.0	1301.6	1351.0	1200.0	1300.0	1350.0
Kidneys	326.4	439.0	299.0	310.0	422.0	289.1	371.0	275.0	275.0	357.0
Liver	1800.4	2362.0	1910.0	1800.0	2360.0	1397.9	1811.0	1400.0	1400.0	1810.0
Pancreas	139.5	173.0	94.0	140.0	174.0	119.9	145.0	85.0	120.0	145.0
Spleen	150.3	229.0	183.0	150.0	228.0	129.9	188.0	150.0	130.0	187.0
Thymus	25.1	25.0	21.0	25.0	26.0	20.1	20.0	20.0	20.0	21.0
Thyroid	20.0	23.0	21.0	20.0	23.0	17.0	19.0	17.0	17.0	20.0

to the difference in organ mass between the ORNL stylized phantoms used in OLINDA and the NCI hybrid phantoms in NCINM as shown in table 4. On the contrary, self-absorption SAFs did not show much difference between NCINM and IDAC 2.1 since both programs adopt the phantoms matching reference data from ICRP. More differences were observed among NCINM, OLINDA/EXM 1.0 and IDAC 2.1 for cross-irradiation SAFs mainly due to the inter-phantom anatomical variability. The largest differences systematically observed between the thymus and thyroid for the 15-year-old and adult phantoms can be explained by the unrealistic distance between thymus and thyroid in the ORNL phantoms, which was also reported by Smith *et al* (Smith *et al* 2001).

Large differences were also observed in S value comparisons between NCINM and OLINDA/EXM 1.0, which is a direct consequence of the differences observed in SAFs. Very similar trends were observed for different radionuclides despite their different emission properties (figure 3(A)). No clear dependency on age was observed from the ratios of the S values from OLINDA/EXM 1.0 to NCINM, except that the difference was slightly greater for the 1-year-old phantoms compared to the other ages (figure 3(B)). Absorbed dose coefficients for adult phantoms showed greater discrepancies between NCINM and OLINDA/EXM 1.0 than between NCINM and IDAC 2.1. For example, a roughly two-fold difference was observed in absorbed dose coefficients to the adrenals between OLINDA/EXM 1.0 and NCINM for the adult male phantom in the case of ^{111}In-DTPA-octreotide, ^{99m}Tc-MAG3 and ^{99m}Tc-ECD. The differences between NCINM and IDAC 2.1 were smaller than between OLINDA/EXC 1.0 and NCINM but still noticeable for adult phantoms, which originates from the inter-phantom anatomical variability: NCI phantoms versus ICRP reference voxel phantoms.

The authors acknowledge following limitations and future improvement needs. First, the current version of NCINM is not designed for dosimetry in nuclear medicine procedures for cancer treatment. There is no feature available for users to define tumor volumes within the target organs. This feature should be of interest for model-based dosimetry in Targeted Radionuclide Therapy (TRT) in the absence or in complement of patient-specific dosimetry. Second, we did not include SAFs from alpha particles in the current version of NCINM. As Targeted Alpha-particle Therapy (TAT) is rapidly developing using alpha particle-emitting isotopes such as ^{211}At, ^{213}Bi, ^{223}Ra and ^{225}Ac (Dekempeneer *et al* 2016), implementation of alpha-particle SAFs into NCINM will allow for broader applications. Lastly, in the current version, users must input pre-calculated residence times (or cumulated activities). In clinical dosimetry applications, a preliminary step for users would involve the curve fitting of time-activity curves for each source organ, which can be obtained from the activity quantification on functional images at different time periods after administration. In epidemiological studies, residence times are most likely to be obtained from the literature. This data input could be facilitated by a biokinetic module providing curve fitting tools and pre-existing biokinetic data collected from literature.

Despite these limitations and further development needs, NCINM can be a valuable asset to the nuclear medicine community: it not only enables state-of-the-art internal dosimetry calculations but also allows for direct quantification of dose uncertainty caused by interpatient anatomical variability, which is reported to have a large impact on absorbed doses in nuclear medicine. We are aware that the model-based dosimetry still has limitations for estimating patient-specific dose. Efforts are currently being made towards more patient specificity through different approaches such as age scaling and body size adjustments.

5. Conclusion

We developed a novel model-based dosimetry tool, NCINM, for patients undergoing nuclear medicine procedures by using a series of pediatric and adult computational phantoms matching ICRP reference data combined with Monte Carlo radiation transport methods. Users can calculate absorbed doses delivered to 55 target regions from 68 source regions within 12 pediatric and adult phantoms for 299 radionuclides using a graphical user interface-based computer program performing on different major operating systems. We observed that internal dosimetry quantities including SAFs, S values, and absorbed dose coefficients are greatly dependent on the type of computational human phantoms, with notable differences observed between the tools based on old phantoms and NCINM, and a reasonable agreement observed between a newer tool based on ICRP reference phantoms and NCINM. The next version of our dosimetry tool will incorporate alpha SAFs and ICRP biokinetic models. NCINM should be a useful tool for epidemiological and clinical dosimetry studies of diagnostic nuclear medicine procedures. NCINM is available for research purposes free of charge from http://ncidose.cancer.gov.

Acknowledgments

This research was funded by the intramural research program of the National Institutes of Health (NIH), National Cancer Institute, Division of Cancer Epidemiology and Genetics. This work utilized the computational resources of the NIH High-Performance Computing Biowulf cluster (http://biowulf.nih.gov).

ORCID iDs

Daphnée Villoing https://orcid.org/0000-0003-1437-2211
Thomas A Cuthbert https://orcid.org/0000-0002-5351-369X
Cari M Kitahara https://orcid.org/0000-0001-6416-4432
Choonsik Lee https://orcid.org/0000-0003-4289-9870

References

Andersson M, Johansson L, Minarik D, Mattsson S and Leide-Svegborn S 2014 An internal radiation dosimetry computer program, IDAC 2.0, for estimation of patient doses from radiopharmaceuticals *Radiat Prot Dosimetry* **162** 299–305

Botta F *et al* 2013 Use of the FLUKA Monte Carlo code for 3D patient-specific dosimetry on PET-CT and SPECT-CT images *Phys. Med. Biol.* **58** 8099–120

Chao T C and Xu X G 2001 Specific absorbed fractions from the image-based VIP-Man body model and EGS4-VLSI Monte Carlo code: internal electron emitters *Phys. Med. Biol.* **46** 901–27

Chiavassa S, Aubineau-Lanièce I, Bitar A, Lisbona A, Barbet J, Franck D, Jourdain J R and Bardiès M 2006 Validation of a personalized dosimetric evaluation tool (Oedipe) for targeted radiotherapy based on the Monte Carlo MCNPX code *Phys. Med. Biol.* **51** 601–16

Cristy M 1980 *Mathematical Phantoms Representing Children of Various Ages for Use in Estimates of Internal Dose* (Oak Ridge, TN: Oak Ridge National Laboratory)

Dekempeneer Y, Keyaerts M, Krasniqi A, Puttemans J, Muyldermans S, Lahoutte T, D'huyvetter M and Devoogdt N 2016 Targeted alpha therapy using short-lived alpha-particles and the promise of nanobodies as targeting vehicle *Expert. Opin. Biol. Ther.* **16** 1035–47

Drozdovitch V *et al* 2015 Use of radiopharmaceuticals in diagnostic nuclear medicine in the United States *Health Phys.* **108** 520–37

Eckerman K F and Endo A 2008 *MIRD: Radionuclide Data and Decay Schemes* (Reston, VA: Society for Nuclear Medicine)

Gutfilen B and Valentini G 2014 Radiopharmaceuticals in nuclear medicine: recent developments for SPECT and PET studies *Biomed. Res. Int.* **2014** 426892

Hung G-U, Wang Y-F, Su H-Y, Hsieh T-C, Ko C-L and Yen R-F 2016 New trends in radionuclide myocardial perfusion imaging *Acta. Cardiol. Sin.* **32** 156–66

ICRP 1988 Radiation dose to patients from radiopharmaceuticals *ICRP Publication 53. Ann. ICRP* **18** 1–4

ICRP 1991 1990 recommendations of the international commission on radiological protection *ICRP publication 60, Ann. ICRP* **21** 1–201

ICRP 1998 Radiation dose to patients from radiopharmaceuticals (addendum to ICRP publication 53). ICRP publication 80 *ICRP Publication 80. Ann. ICRP* **28** 1–126

ICRP 2002 Basic anatomical and physiological data for use in radiological protection : reference values *ICRP publication 89, Ann. ICRP* **32** 5–265

ICRP 2006 Human alimentary tract model for radiological protection *ICRP publication 100, Ann. ICRP* **36** 25–327

ICRP 2007 The 2007 recommendations of the international commission on radiological protection *ICRP publication 103, Ann. ICRP* **37** 1–332

ICRP 2008a Nuclear decay data for dosimetric calculations *ICRP publication 107. Ann. ICRP* **38** 7–96

ICRP 2008b Radiation dose to patients from radiopharmaceuticals - addendum 3 to ICRP publication 53 *ICRP Publication 106. Ann. ICRP* **38** 1–197

ICRP 2009 Adult Reference Computational Phantoms *ICRP Publication 110, Ann. ICRP* **39** 1–164

ICRP 2016 The ICRP computational framework for internal dose assessment for reference adults: specific absorbed fractions *ICRP Publication 133. Ann. ICRP* **45** 1–74

ICRU 1992 *Photon, Electron, Proton and Neutron Interaction Data for Body Tissues* (Bethesda, MD: International Commission on Radiation Units and Measurements)

Johansson L 1985 *Patient Irradiation in Diagnostic Nuclear Medicine: Assessment of Absorbed Dose and Effective Dose Equivalent Dosimetry* (Gothenburg, Sweden: Gothenburg University)

Johnson P B, Bahadori A A, Eckerman K F, Lee C and Bolch W E 2011 Response functions for computing absorbed dose to skeletal tissues from photon irradiation - an update *Phys. Med. Biol.* **56** 2347–65

Kitahara C M *et al* 2019 Association of radioactive iodine treatment with cancer mortality in patients with hyperthyroidism *JAMA Intern. Med.* **179** 1034–1042

Lamart S, Bouville A, Simon S L, Eckerman K F, Melo D and Lee C 2011 Comparison of internal dosimetry factors for three classes of adult computational phantoms with emphasis on I-131 in the thyroid *Phys. Med. Biol.* **56** 7317–35

Lamart S, Simon S L, Bouville A, Moroz B E and Lee C 2016 S values for 131I based on the ICRP adult voxel phantoms *Radiat. Prot. Dosim.* **168** 92–110

Lee C, Lodwick D, Hurtado J, Pafundi D, Williams J L and Bolch W E 2010 The UF family of reference hybrid phantoms for computational radiation dosimetry *Phys. Med. Biol.* **55** 339–63

Lee C, Park S and Lee J K 2007 Specific absorbed fraction for Korean adult voxel phantom from internal photon source *Radiat. Prot. Dosim.* **123** 360–8

Loevinger R, Budinger T F, Thomas F and Watson E E 1991 *MIRD Primer for Absorbed Dose Calculations Revised Edition* (New York: Society of Nuclear Medicine)

Marcatili S, Villoing D, Mauxion T, McParland B J and Bardiès M 2015 Model-based versus specific dosimetry in diagnostic context: comparison of three dosimetric approaches *Med. Phys.* **42** 1288–96

Maurer A H 2008 Combined imaging modalities: PET/CT and SPECT/CT *Health Phys.* **95** 571–6

Melo D R, Brill A B, Zanzonico P, Vicini P, Moroz B, Kwon D, Lamart S, Brenner A, Bouville A and Simon S L 2015 Organ dose estimates for hyperthyroid patients treated with 131I: an update of the thyrotoxicosis follow-up study *Radiat. Res.* **184** 595–610

NCRP 2009 *Report No. 160, Ionizing Radiation Exposure of the Population of the United States* (Bethesda, MD: National Council on Radiation Protection and Measurements)

NCRP 2019 *Report No. 184, Medical Radiation Exposure of Patients in the United States* (Bethesda, MD: National Council on Radiation Protection and Measurements)

Pelowitz D B 2011 *MCNPX user's manual Version 2.7.0* Los Alamos National Laboratory

Petitguillaume A, Bernardini M, Broggio D, Vaylet C D L, Franck D and Desbrée A 2014 OEDIPE, a software for personalized Monte Carlo dosimetry and treatment planning optimization in nuclear medicine: absorbed dose and biologically effective dose considerations *Radioprotection* **49** 275–81

Petoussi-Henss N, Bolch W E, Zankl M, Sgouros G and Wessels B 2007 Patient-specific scaling of reference S-values for cross-organ radionuclide S-values: what is appropriate? *Radiat. Prot. Dosim.* **127** 192–6

Ron E *et al* 1998 Cancer mortality following treatment for adult hyperthyroidism. Cooperative thyrotoxicosis therapy follow-up study group *JAMA.* **280** 347–55

Smith T J, Phipps A W, Petoussi-Henss N and Zankl M 2001 Impact on internal doses of photon SAFs derived with the GSF adult male voxel phantom *Health Phys.* **80** 477–85

Snyder W S, Ford M R, Warner G G and Watson E E 1975 *MIRD Pamphlet No. 11 (revised): 'S' Absorbed Dose Per Unit*

Cumulated Activity for Selected Radionuclides and Organs (New York, NY: Society of Nuclear Medicine)
Stabin M and Farmer A 2012 OLINDA/EXM 2.0: the new generation dosimetry modeling code *J. Nucl. Med.* **53** 585–585
Stabin M G 1996 MIRDOSE: personal computer software for internal dose assessment in nuclear medicine *J. Nucl. Med.* **37** 538–46
Stabin M G, Sparks R B and Crowe E 2005 OLINDA/EXM: the second-generation personal computer software for internal dose assessment in nuclear medicine *J. Nucl. Med.* **46** 1023–7
Xu X G 2014 An exponential growth of computational phantom research in radiation protection, imaging, and radiotherapy: a review of the fifty-year history *Phys. Med. Biol.* **59** R233–302
Yoriyaz H, Stabin M G and dos Santos A 2001 Monte Carlo MCNP-4B-based absorbed dose distribution estimates for patient-specific dosimetry *J. Nucl. Med.* **42** 662–9
Zankl M, Petoussi-Henss N, Fill U and Regulla D 2003 The application of voxel phantoms to the internal dosimetry of radionuclides *Radiat. Prot. Dosimetry* **105** 539–48